Soil Dynamics and Earthquake Engineering 157 (2022) 107251

Contents lists available at ScienceDirect

Soil Dynamics and Earthquake Engineering

journal homepage: www.elsevier.com/locate/soildyn

Experimental investigation of transient bending moment of piles during seismic liquefaction

M. Rouholamin [a], D. Lombardi [b], S. Bhattacharya [c,*]

[a] Geotechnical Engineering, University of Portsmouth, School of Civil Engineering and Surveying, Portsmouth, PO1 3AH, UK
[b] University of Manchester, School of Mechanical, Aerospace & Civil Engineering, Manchester, UK
[c] Geomechanics, University of Surrey, Department of Civil and Environmental Engineering, Guildford, Surrey, GU2 7XH, UK

A R T I C L E I N F O

Keywords:
Liquefaction
Pile
Earthquake
Transient bending moment
Shaking table

A B S T R A C T

The purpose of this paper is to study the behavior of pile-supported structures in liquefiable soils, specifically when the soil surrounding the pile transits from no-liquefaction to full-liquefaction. A series of shaking table tests were performed on four pile-supported structures subjected to different input motions and, as a result, with different times to reach full-liquefaction. The bending moment of the piles during the transient phase is compared with those predicted in pre- and post-liquefaction stages. The experimental results showed that the maximum bending moment may occur during the transient phase (i.e. during the development of excess pore pressure before the soil is fully liquefied). Arguably, the observed amplification in bending moment is caused by the the tuning effect between the predominant frequency of the input motion and the frequency of the pile-supported structure, which is progressively decreasing during the liquefaction process. Results are presented using a non-dimensional framework whose parameters are derived from the governing mechanics. A new parameter TAF (Transient Amplification Factor) is defined to predict the design bending moment during the transient phase. It is shown that the transient bending moment can be obtained from the newly introduced parameter TAF, and the values of maximum bending moments in the pre- and post-liquefaction stages. It is found that TAF is a function of two easily obtainable parameters: (a) time taken to reach full liquefaction, this can be obtained through site response analysis; (b) elongation of natural period of vibration, expressed as ratio of the time period of the structure at full liquefaction to the time period at zero-liquefaction. Finally, practical implications of the main findings are discussed.

1. Introduction

The dynamic behaviour of pile-supported structures founded in liquefiable deposits is still an area of active research [1–30] due to the poor performance of piled foundations as observed in most of the recent earthquakes [9,31]. The current methods of pile design - see for Example codes of practices such as JRA [32,33] NEHRP [34], IS-1893 [35], focus on avoiding bending, buckling and settlement failures. The effect of dynamic soil-structure-interaction (SSI) effects is taken into account by means of empirical correlations.

Fig. 1 shows the two main stages of loading in a typical pile-supported structure during an earthquake. Fig. 1 (a) shows the stage at the start of the shaking, before any build-up of the excess pore water pressure takes place. In this stage, piles are mostly subjected to inertia loads induced by the ground shaking and oscillation of the superstructure. It is known that inertia loads tend to generate high bending moments at relatively shallow depths along the pile. Fig. 2 (a) shows the “Beam on Non-Linear Winkler Foundation" model, in which the effect due to soil-structure interaction is modelled by a set of springs distributed at discrete locations along the length of the pile. Each spring is defined by a relationship between the soil pressure (p) and pile deflection (y) referred to as p-y curve. This method is conventionally used to compute the internal forces (i.e. bending moment and shear force) and pile’s deflection. The typical shape of p-y curves for sand in non-liquefied condition is shown in Fig. 2 (b), and further details can be found in API [36]. However, in saturated loose to medium dense sand, the ground shaking induce a gradual increase in pore water pressure, resulting in the soil to progressively lose its strength and stiffness. When the excess pore pressure equalises the overburden pressure, the soil is said to be in a full-liquefaction condition; at full liquefaction the

* Corresponding author. Geomechanics, Department of Civil and Environmental Engineering University of Surrey, GU2 7XH, UK.
E-mail address: S.Bhattacharya@surrey.ac.uk (S. Bhattacharya).

https://doi.org/10.1016/j.soildyn.2022.107251
Received 25 August 2021; Received in revised form 3 March 2022; Accepted 10 March 2022
Available online 25 March 2022

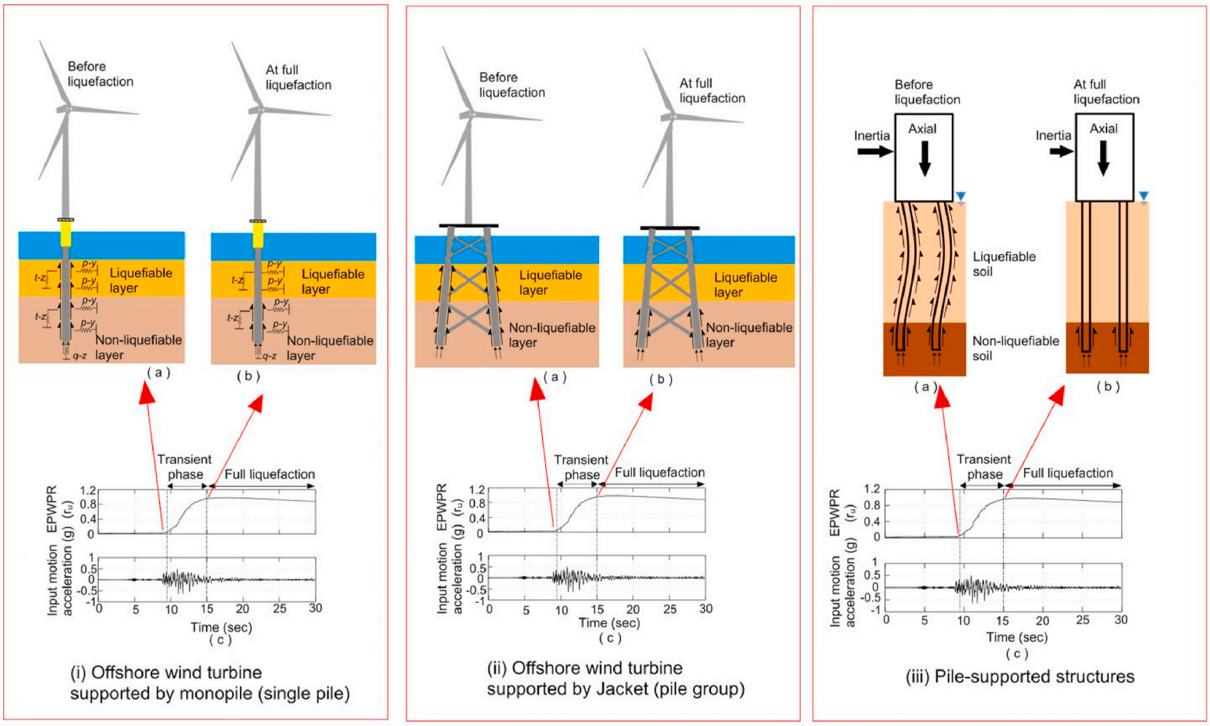

Fig. 1. Schematic of loading conditions acting on a typical offshore wind turbine foundations (i) monopile, (ii) jacket and (iii) pile supported structures in seismically liquefiable soils: (a) before liquefaction; (b) at fully liquefaction; (c) typical input motion time history and corresponding excess pore water pressure ratio profile).

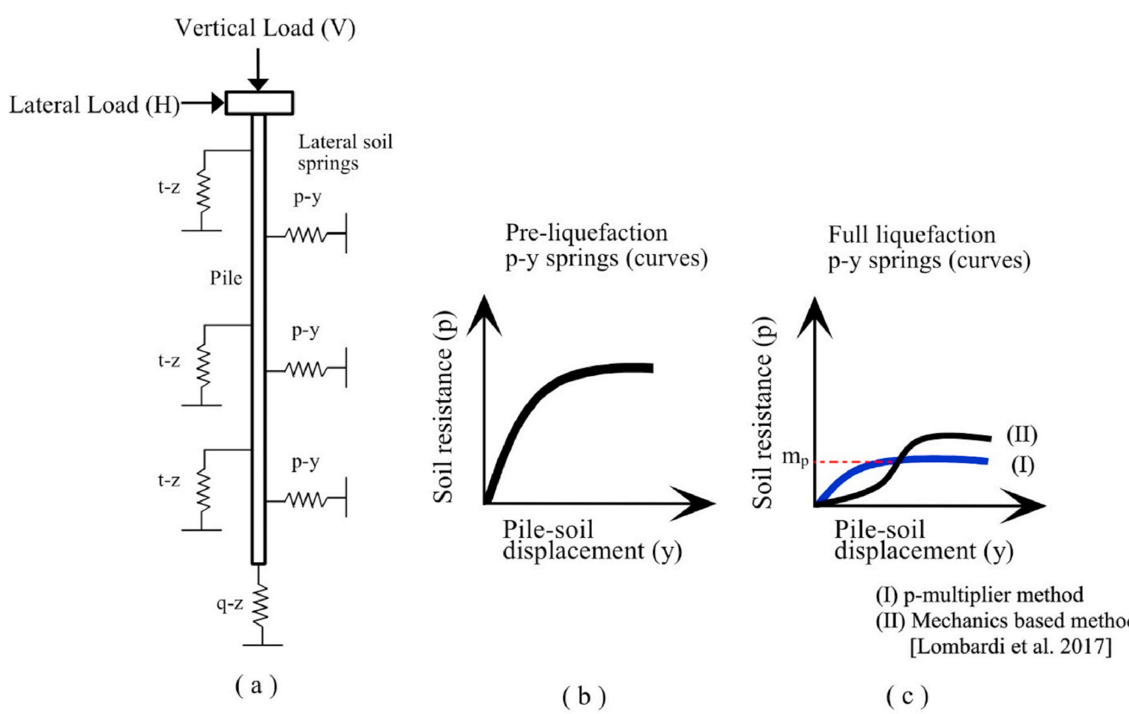

Fig. 2. (a) Beam on Non-Linear Winkler Foundation" model, (b) pre liquefaction p-y curves & (c) post liquefaction p-y curves.

foundation loses the support from its sorrounding soil and the piles tend to act as an unsupported column over the liquefied layer, see Refs. [37, 38]. Fig. 1c shows the time history of a real earthquake together with excess pore water pressure profile, which can be either measured in experiments or computed by means of site response analyses. From the figure it can be noted that the onset of liquefaction occurs in a finite amount of time, whose duration depends mostly on the input motion characteristics and the density of the soil; the latter is typically expressed in terms of relative density. Typical values of time to reach liquefaction range between 6 and 15s, however, the actual time can be estimated by means of nonlinear finite element analysis. During the process of excess pore pressure build-up, referred to as transient by Lombardi and Bhattacharya [9], the inertial load applied to the pile head reduces due to the combined effects of lengthening in natural period of the structure and

Table 1
Index properties of Redhill 110 sand [46].

Specific gravity, G_s	D_{50} [mm]	Maximum void ratio, e_{max}	Minimum void ratio, e_{min}	Critical angle of friction φ_c, [°]
2.65	0.18	1.035	0.608	36

increase in damping of the liquefied soil. The transition from no liquefaction to full liquefaction takes a finite time, during which the pile experiences temporal and spatial variation of maximum bending moments. At full liquefaction, the bending moment envelopes can be obtained using the Winkler approach, with the p-y curves shown in Fig. 2c, which differently from the convetional p-y curves, take into account the tendency of the liquefied soil to dilate upon shearing [38]; it is worth noting that, at this stage, the structure is subjected to a different inertial load due to the lengthning in vibration period caused by liquefaction. It may be noted that there are two types of p-y curves (referred to as I and II in Fig. 2c) for liquefied soil as shown in Fig. 2c. Curve type I is constructed according to the *p-multiplier* method [39,40], where a reduction factor, known as "p-multiplier" (m_p), is used to obtain the empirical p-y curves for liquefied soil from its non-liquefied counterpart. The reduction factor m_p ranges typically from 0.01 to 0.1 [41,42]. On the other hand, Curve II is derived from a mechanics-based approach, and it has the advantage of taking into account the actual stress-strain behaviour of liquefied soil as observed in element tests [43,44]; Dash, 2010 [45,46]; and physical model tests [8,47,48]. Dash et al. [49] sets out a practical method to construct curve II taking as input parameter the initial relative density of the soil in its pre-liquefied condition.

The previous methods can be used by practitioners to determine the maximum bending moment after the onset of liquefaction; yet bending moments can be significantly higher during the transition to liquefaction due to the resonance effects triggered by the lengthening in period of the structure. Such bending moments cannot be predicted with the available methods, and there is no general consensus on what the amplification factor should be applied to the bending moments. Therefore, in order to investigate the transient behaviour of pile-supported structures, and its implication on the overall seismic response of these structures, a series of large shaking table tests have been performed on four models representing typical pile-supported structures. Specifically, the effects of time to reach liquefaction, and characteristics of the input motion (i.e. frequency content and amplitude) on mechanical characteristics of the models are investigated. The aim and scope of the paper are as follows:

(a) To describe the shaking table tests and investigate the transient behaviour of four pile-supported structures subjected to different types of input motion, and consequently different duration of the transient phase.
(b) To present the experimental results using a non-dimensional framework that enable the analysis of the complex dynamic behaviour of piled foundations during the transient phase.

2. Physical modelling of transient pile-soil interaction

2.1. Shaking table, soil and model container

The experimental programme was carried out at normal gravity using the shake table facility at the BLADE (Bristol Laboratory for Advanced Dynamics Engineering). The shake table consisted of a 3 × 3 m cast aluminium platform driven by eight servo hydraulic actuators that allowed full control of motion in six degrees of freedom. The soil container consisted of a rigid box with absorbing boundaries having the dimensions of 2.40 m long, 1.2 m wide, and 2.4 m high. Absorbing boundaries were used to mitigate the unwanted reflection of body waves and minimise other dynamic boundary effects. Further details on the box and criteria for selection of the absorbing material is provided in

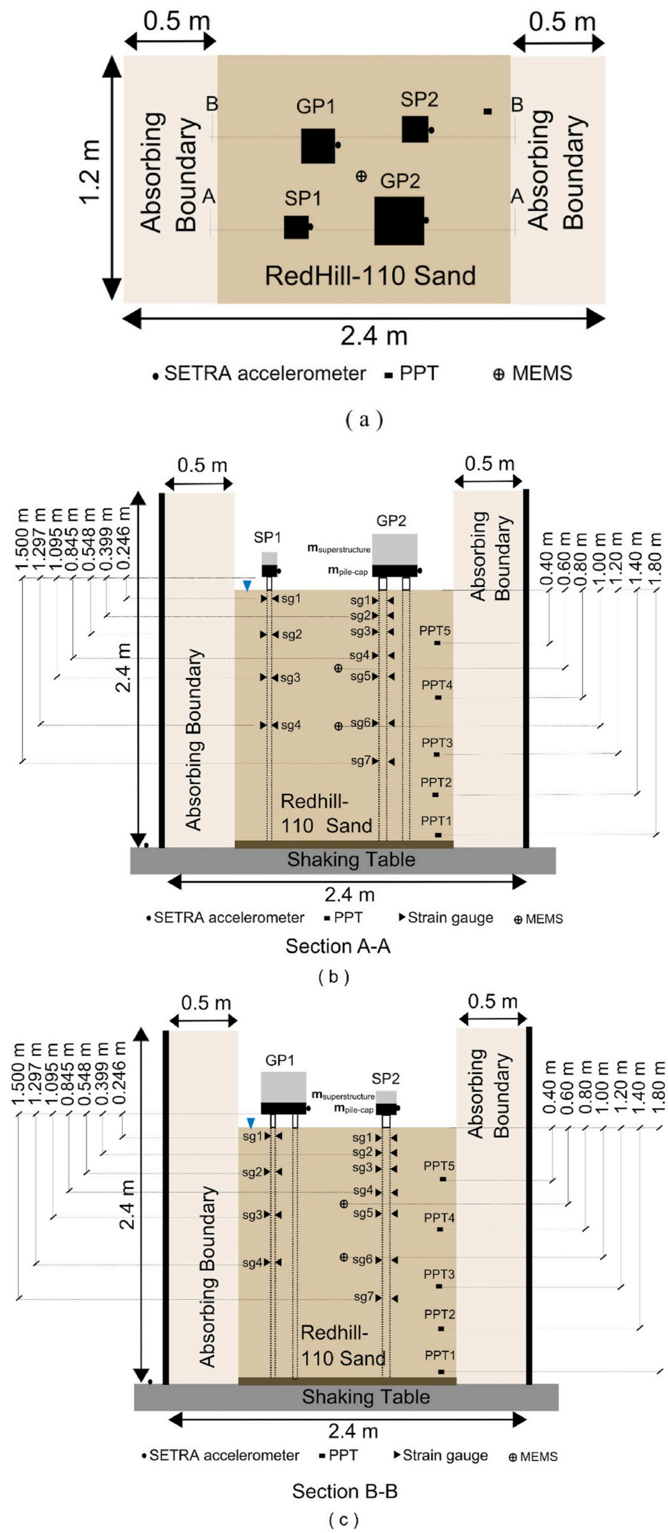

Fig. 3. Schematic view and the instrument location of the shaking table test: (a) plan view (b) & (c) side view.

Lombardi et al. [50] and Bhattacharya et al. [51]. The sand deposit consisted of a relatively uniform layer of Redhill 110 sand, whose index properties are listed in Table 1. Soil homogeneity was achieved by pluviating dry sand from a constant height of fall of 1.5 m and by using flexible tube 50 mm in diameter. Saturation of the soil deposit was carried out from top to bottom and the saturation process was monitored through pore pressure transducers at 5 different depths as shown in

Table 2
Mechanical characteristics of pile models used in the experiment.

Model ID	*Outer Diameter* [mm]	*Wall thickness [mm]*	*Pile length [m]*	*Spaces between piles [mm]*	*EI* [Nm^2]	$m_{pile\text{-}cap}$ [kg]	$m_{superstructure}$ [kg]	M_y [Nm]	M_p [Nm]	P/P_{cr}	P/P_{cr} *Based on Tang* et al. *(2019)*
SP1	25.4	0.711	2	N/A	294	1.9	5	58	74	0.38	0.6
SP2	41.3	0.711	2	N/A	1305	8.44	20	156	199	0.42	2.5
GP1	25.4	0.711	2	76.2	294	13.08	65	58	74	0.20	1.7
GP2	41.3	0.711	2	123.9	1305	22.72	115	156	199	0.20	3.0

D is outer diameter; *EI* is bending rigidity; $m_{pile\text{-}cap}$ is mass of pile-cap; $m_{superstructure}$ is mass of superstructure; M_y *is Y*ield moment capacity; M_p is plastic moment capacity; P/P_{cr} ratio of Axial load to Critical load.

Table 3
Test programme and Input motion properties applied on the structures.

Test ID	Input	PA [g]	t_{liq} [s]	Model tested	Remarks
WN-1	White noise – frequency range 0–100 Hz of total 300s duration	0.15	50	SP1, SP2, GP1 and GP2	These tests were carried out to evaluate the dynamic characteristics of the systems over a long transition phase time
CH-1	2011 Christchurch earthquake* (0.5)	0.63	4	SP1	SP1 failed. Other models didn't have any superstructure mass
CH-2	2011 Christchurch earthquake* (1.3)	1.70	4.5	SP2	SP2 failed. This is the last test and other models (SP1, GP1 and GP2) failed.
CH-3	2011 Christchurch earthquake * (0.7)	0.92	6	GP1	GP1 failed. Before this test, SP1 and GP2 failed. SP2 did not have any superstructure mass
CH-4	2011 Christchurch earthquake * (0.7)	0.92	4	GP2	GP2 failed. Before this test SP1 failed and GP1 and SP2 didn't have any superstructure mass.
CH-5	2011 Christchurch earthquake * (1)	1.53	6	SP2	Before this test SP1, GP1 and GP2 failed. In this test SP2 did not fail.
CH-6	2011 Christchurch earthquake * (0.5)	0.63	5	GP1	Before this test, SP1 and GP2 failed. In this test GP1 did not fail and SP2 did not have any superstructure mass
CH-7	2011 Christchurch earthquake* (0.5)	0.63	4	GP2	Before this test SP1 failed and GP1 and SP2 didn't have any superstructure mass. In this test GP2 did not fail.
IR-1	1980 Irpinia earthquake	0.25	6	SP2	Before this test SP1, GP1 and GP2 failed. In this test SP2 did not fail.
FR-1	1976 Friuli earthquake	0.35	3	SP2	Before this test SP1, GP1 and GP2 failed. In this test SP2 did not fail.
AQ-1	2009 L'Acquila earthquake	0.32	7	SP2	Before this test SP1, GP1 and GP2 failed. In this test SP2 did not fail.

PA = Peak input acceleration applied at the base; t_{liq} is time required to achieve full liquefaction; *scaled factor of the input motion where scale factor is given between brackets.

Fig. 3. The average relative density of the soil is about 34% and details can be found in Rouholamin [52].

2.2. Pile-supported structures and instrumentation

The physical models consisted of four pile-supported structures, representing two single piles and two 2 × 2 pile-supported structures (see Fig. 3). These are hereafter referred to as SP1 and SP2 (single pile 1 and 2, respectively) and GP1 and GP2 (pile group 1 and 2, respectively). Piles were 2 m long aluminium alloy tubes and many of the properties are given in Table 2. As shown in Fig. 3, each model had a steel pile-cap where superstructure mass can be attached. All piles were rigidly connected to a bottom plate to ensure full fixity, a condition that can be considered valid for piles penetrating into a firm non-liquefiable soil layer. In the pile-group models this arrangement allowed free translational movements of the pile-cap but no relative rotations between the piles. Dimensions and mechanical properties of the models are listed in Table 2. For each model, the table also lists the ratio of applied axial load (*P*) to Euler Critical load (P_{cr}), the latter being computed considering the piles as unsupported columns i.e. neglecting the presence of soil support. In the table, P/P_{cr} is also calculated based on the method suggested by Tang et al., 2019 where resistance of liquefied soil is also considered. As shown in Fig. 3, piles were instrumented with strain gauges attached at different elevations along the pile. To monitor the model response, pile-caps were equipped with accelerometers (type 141A, manufactured by SETRA). Ground accelerations were monitored by means of MEMS accelerometers (see [53]) The data acquisition system consisted of 4 Microstar Laboratories MSXB028 analog-digital converter (ADC) cards. Data was simultaneously recorded at a sample frequency of 200 Hz, and signal conditioning comprised filtering -using an 80 Hz low pass Butterworth filter, and removal of offset and drift from the recorded signal due to misalignment of the sensors and electrical instability.

2.3. Testing programme

Eleven shaking table tests were carried out and the main characteristics are listed in Table 3. Strong motion records from 4 different earthquakes (1976 Friuli, 1980 Irpinia, 2009 L'Aquila and 2011 Christchurch) were used to simulate different earthquake scenarios so that the responses to different patterns of liquefaction can be studied. White Noise (WN-1 in Table 3) test is used so as provide an unusually longer time to reach full liquefaction together with dynamic motion rich in frequency. In particular, it was intended to observe the response of the pile-supported structures with different patterns of soil liquefaction and purposefully get tuned with earthquake motion. CH1 to CH8 represented 2011 Christchurch earthquake with different amplitudes of magnitude scaling. The superstructures were mounted on the pile-cap of the models in different tests, as detailed in Table 3.

3. Experimental results

3.1. Frequency domain analysis

To quantify the change in vibration characteristics of the models, the

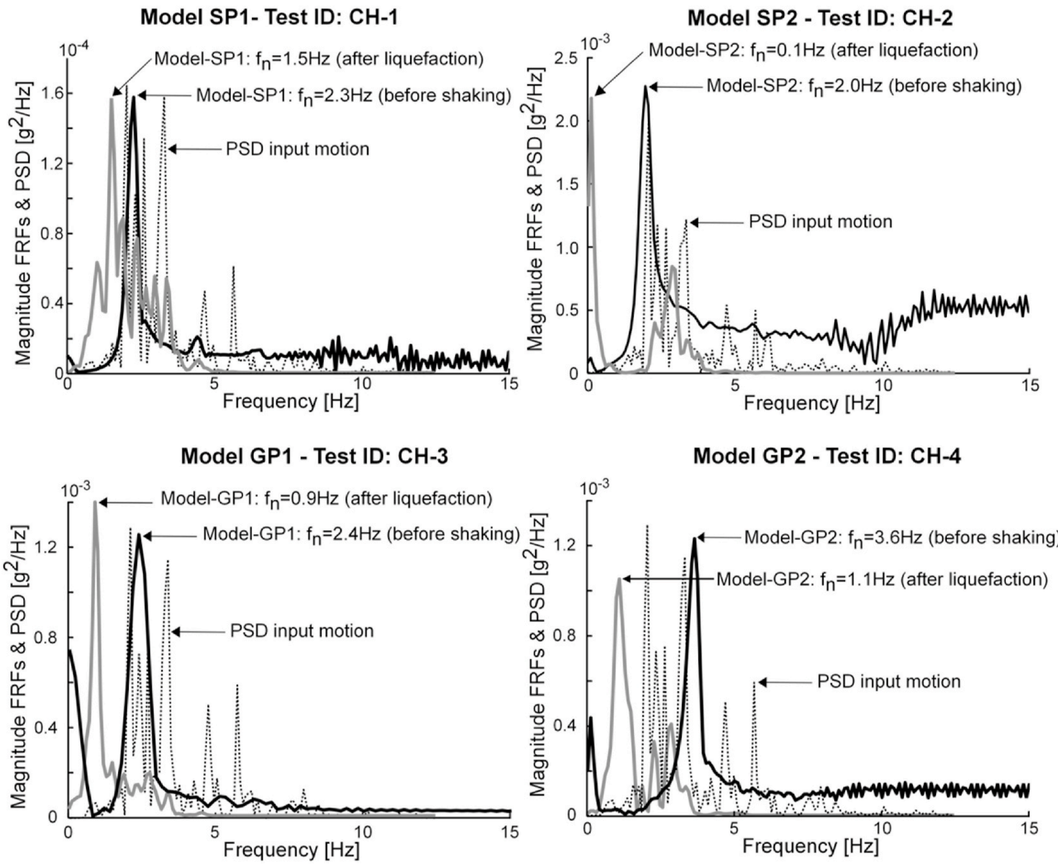

Fig. 4. Comparison of natural frequency of pile models before and at full liquefaction together with the Power Spectrum Density (PSD) of the applied earthquakes. (Test IDs: CH-1; CH-2; CH-3; CH-4).

experimental data was first analysed in frequency domain. Before the start of each test, the natural frequencies of the models were estimated from free vibration tests performed by exciting the structure with an impact hammer. The frequency response functions FRFs obtained from the free vibration tests are depicted in darker lines (denoted by before shaking) in Figs. 4–6. In the same figures, the power spectral density (PSD) of the input motion and FRF estimated after liquefaction is shown for comparison. It may be observed that after liquefaction the natural frequency of the models reduced significantly, which may be attributed to the development of excess pore pressure, and in some cases formation of plastic hinges in the piles. From Table 3 it is interesting to note that the four models failed in tests CH1 to CH4. (see Fig. 4 for frequency response). Other tests listed in Table 3 were carried out to investigate the sole effect of liquefaction on the variation in natural frequency of the models and transient bending moments. In these tests, formation of plastic hinges was deliberately avoided with lower pile-head mass. The results shown in Figs. 5 and 6 indicate that the natural frequency of the models reduced to about half due to subsurface liquefaction. As the model transited from higher to lower frequencies it was likely that the seismic response amplified due to a temporarily matching between natural frequency of the models and predominant frequency of the input motion. This aspect is further investigated in the next section by considering the bending moment time histories along the piles.

3.2. Bending moment of pile models and case studies

Bending moments were computed from strain gauge measurements recorded at different locations along the piles (see Fig. 3). Fig. 7 plots the bending moment time histories at different elevations along the pile, input acceleration recorded on the table, acceleration response time history recorded on the pile-cap and excess pore pressure ratio r_u profiles computed from pressure transducers (see Fig. 3 for instrumentation layout). The latter is conventionally defined as the ratio of the excess pore pressure to the effective vertical stress and can conveniently be used to monitor the propagation of the liquefaction front, which was observed to propagate top-down. The transient condition was defined as the phase when the excess pore pressure started gradually to build up before reaching the full liquefaction condition, corresponding to $r_u \geq 0.95$.

Fig. 8 plots typical bending moment profiles of the pile for three different stages. It can be observed that before any development of excess pore pressure (i.e. pre-liquefaction condition), the conventional beam on non-linear Winkler foundation model, with standard p-y curves (shown in Fig. 2b) can be used to compute the bending moments. Such an approach, however, would be ill-suited for predicting the response during the transient condition phase, since the strength and stiffness of the soil has reduced as a result of the excess pore pressure build-up. An alternative approach is unavailable in the current literature, consequently it represents one of the motivations behind this research. At full liquefaction, where beam on non-linear Winkler foundation model with appropriate p-y curves (Fig. 2c) can be used for computation of the bending moment profile. It should be noted that as the pile behaves as an unsupported beam subjected to both axial and lateral load, potential P-delta effects may amplify the bending moment, and therefore these should be taken into account especially in presence of high axial loads or imperfections.

From Fig. 8, it is clear that the maximum bending moment occurred in the transient phase, possibly due to resonance between the natural period of the piled-supported structure and predominant period of the input motion. Although Fig. 8 plots the results from four tests, it must be mentioned that these were consistent with those obtained in the other tests, whose results can be found in Rouholamin [52].

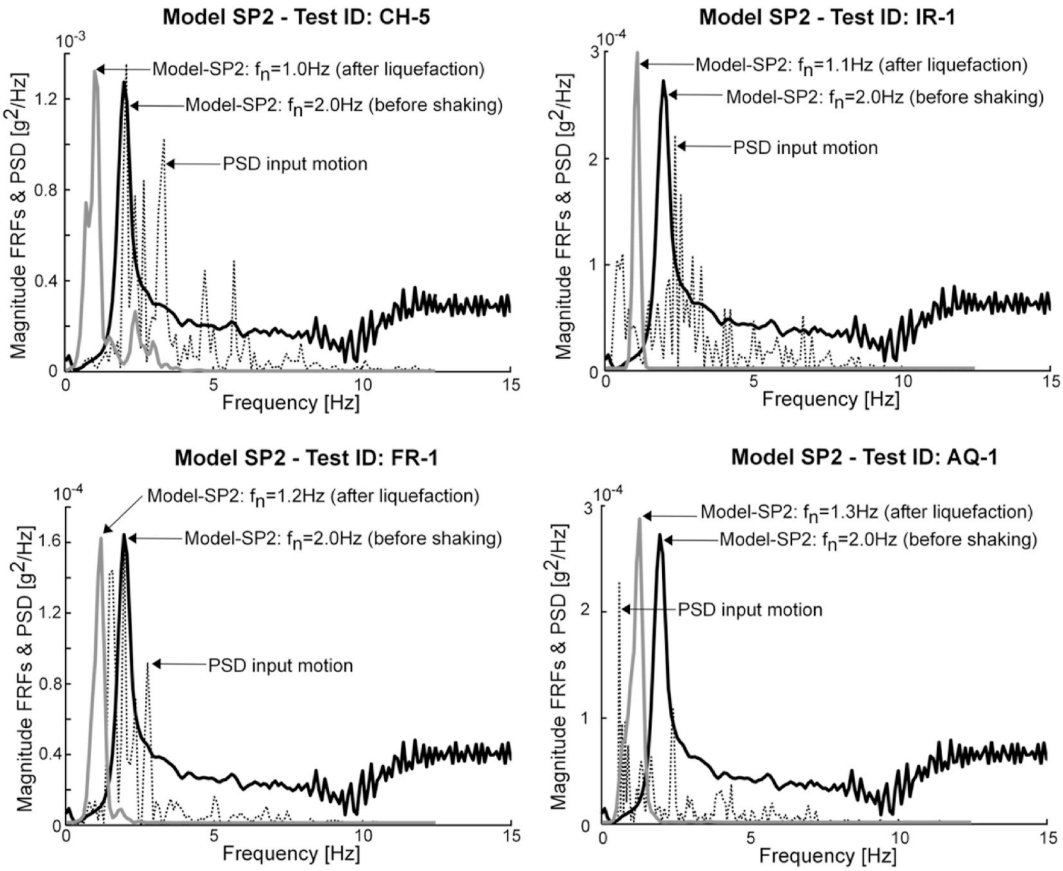

Fig. 5. Comparison of natural frequency of pile models before and at full liquefaction together with the Power Spectrum Density (PSD) of the applied earthquakes (Tests CH-5, IR-1, FR-1, & AQ-1).

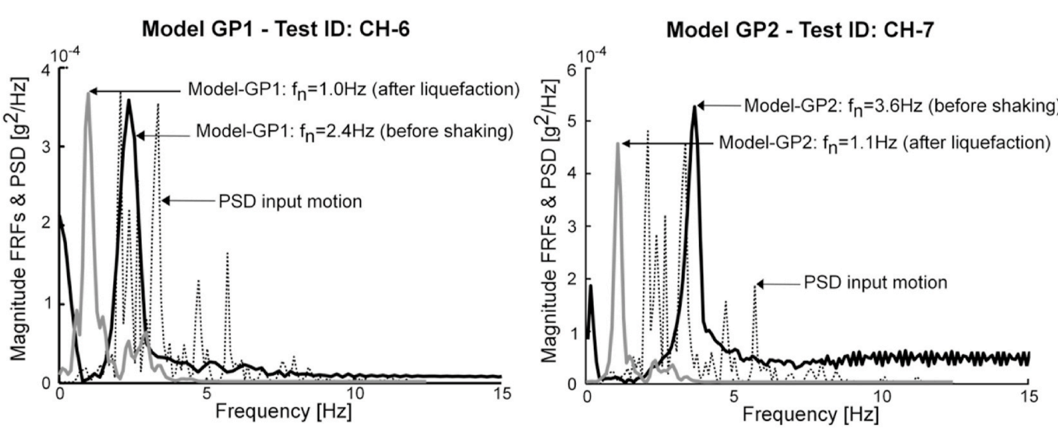

Fig. 6. Comparison of natural frequency of pile models before and at full liquefaction together with the Power Spectrum Density (PSD) of the applied earthquakes (Tests CH-6, CH-7).

To further explore the seismic behaviour of pile-supported structures during the transient phase, it is of interest to reconsider two case studies where a similar response was observed, namely collapse of Showa Bridge after the 1964 Niigata earthquake [54] and response of a 5-storey concrete building in Higashi-Nada, a reclaimed area in Kobe [13]. In the first case, the natural period of Showa Bridge transited from 2s (0.5 Hz) to about 6s (0.16 Hz) as a result of soil liquefaction, which occurred in approximately 10s as reported in Halder et al., [55]. In the second case, the natural period of 5-storey building in Kobe transited from 0.5s (2 Hz) to about 4.5s (0.22 Hz) due to liquefaction, which occurred in approximately 6 s. As typical earthquake frequencies range between 0.5 Hz and 10 Hz, the frequency of the structure is likely to temporarily match with the predominant frequency of the earthquake, resulting in response amplification and consequent amplification of bending moments in the pile.

From Fig. 8, it may be noted that for single pile models (SP1 and SP2) the maximum bending moments occurred at the middle of the liquefied layer, whereas for pile group models, these were recorded in proximity of the pile-heads. It is worth noting that the latter result is expected as due to the boundary conditions of the pile group models discussed in section 2.2. It is worth noting that the distribution of bending moments along the pile computed in the model tests was consistent with the

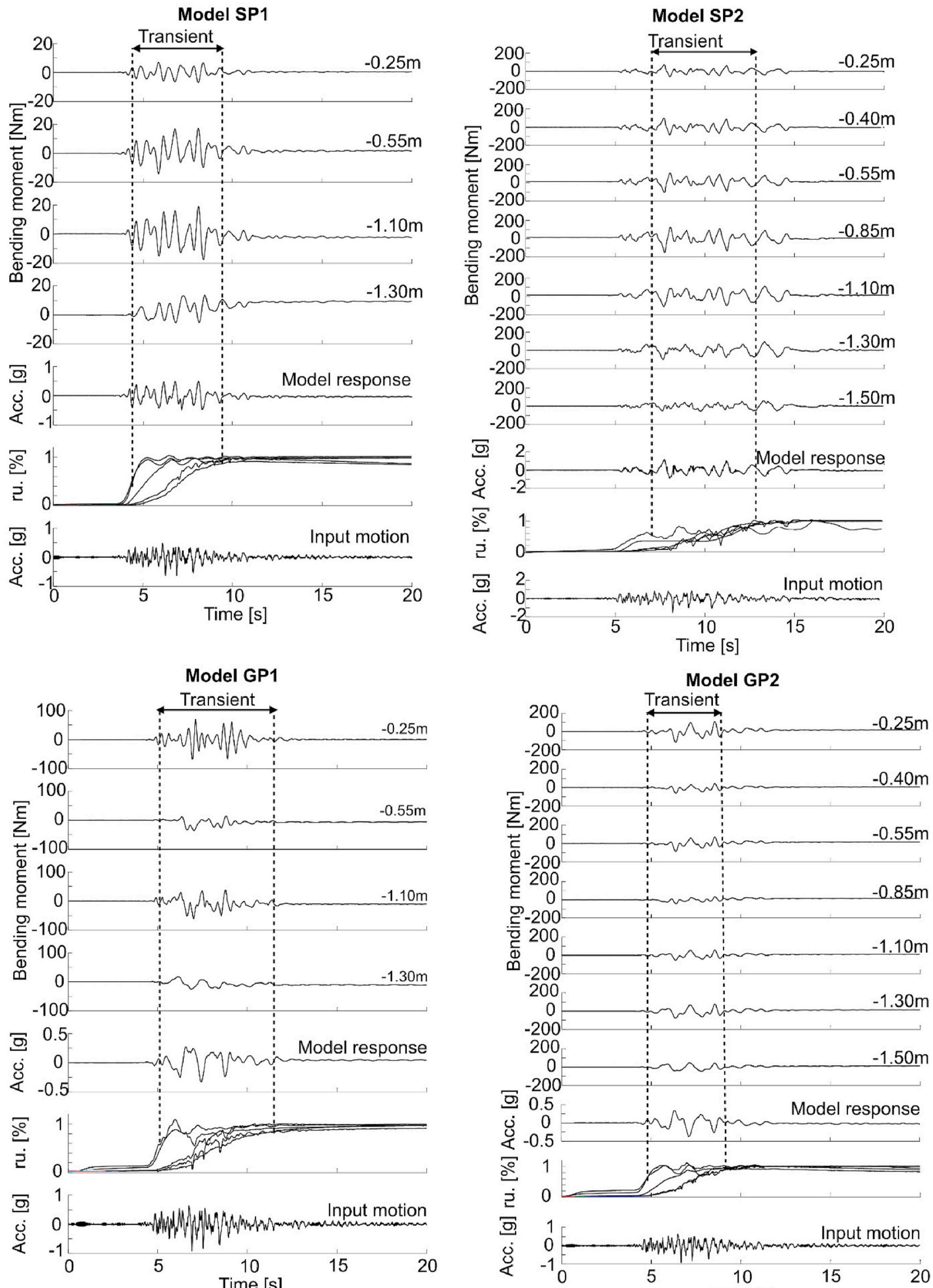

Fig. 7. Bending moment time histories for models SP1 (test ID: CH1), SP2 (test ID: CH5), GP1 (test ID: CH3) and GP2 (test ID CH4). The figure also depicts the excess pore pressure ratio, acceleration response of each model and applied input motion.

damage patterns in piles as observed in post-earthquake reconnaissance missions [56]. In particular, it was observed that plastic hinges occurred not only at the pile head but also in the middle of the liquefied layer. The higher bending moment observed in the transition phase can be attributed to transitory resonance phenomena, also referred to as moving resonance, whose effect can be quantified by means of an appropriate **Transient Amplification Factor** (TAF). As mentioned before, while methods are available to compute pre and post-liquefaction bending moment in the pile through the use of appropriate p-y curves, shown in Fig. 2b and c, respectively, there is no available method to compute the transient bending moment, which as shown earlier, may be larger than the those computed during liquefaction, and thus govern the design.

In order to scale up the model test data acquired through the shake table testing and therefore to predict the prototype's response, it is necessary to introduce some scaling laws. These are presented in Table 4 along with their physical meaning for easy interpretation.

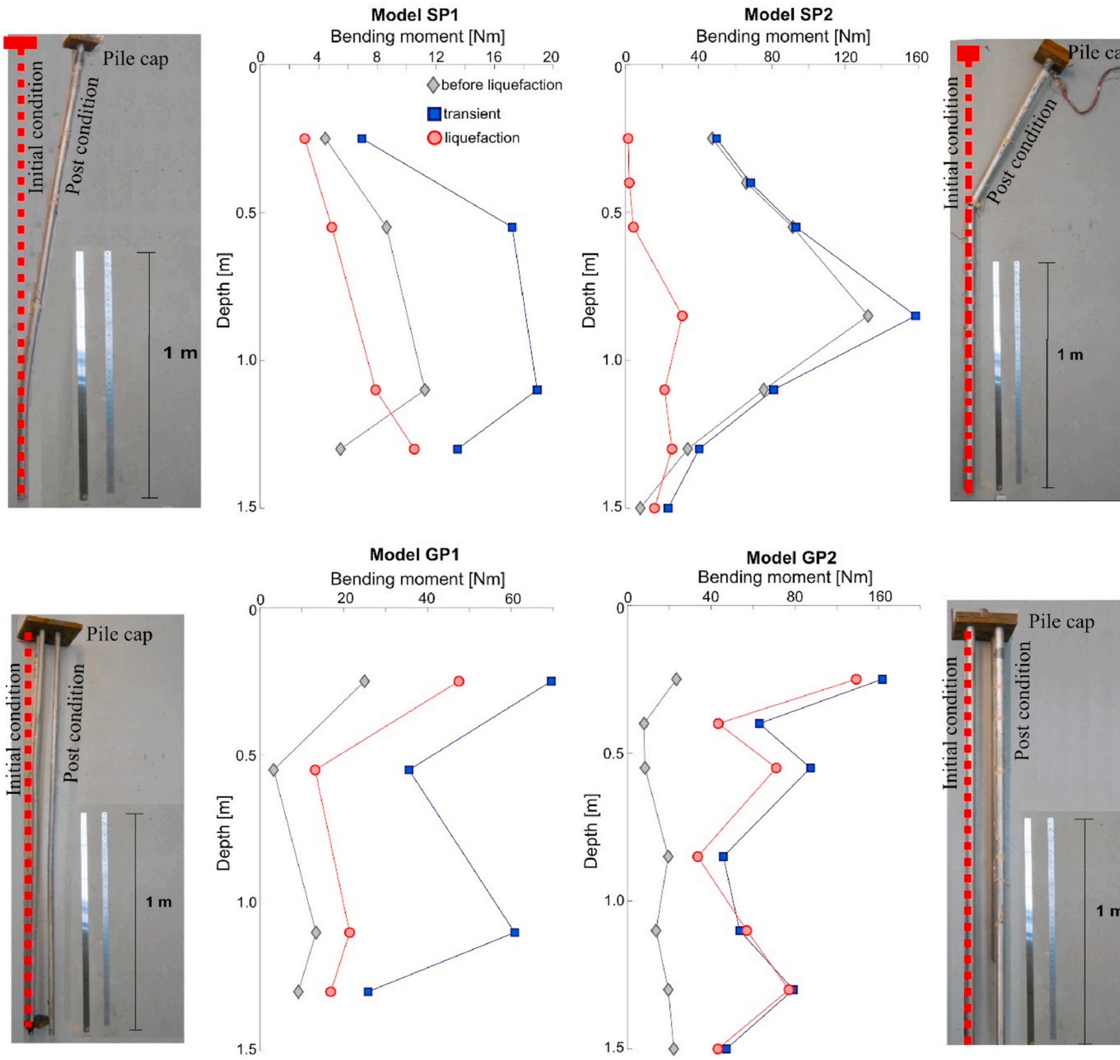

Fig. 8. Bending moment envelopes for models SP1 (test ID: CH1), SP2 (test ID: CH5), GP1 (test ID: CH3) and GP2 (test ID CH4).

The next section defines the **T**ransient **A**mplification **F**actor (TAF) for the pile problem in hand by considering two loading conditions, i.e.: pre- and post-liquefaction conditions. This is intentional as the central aim of the current analysis is to obtain a simplified design rule that designers can use for the assessment of the pre and post-liquefaction bending moments through the application of an appropriate amplification factor, i.e. TAF.

The transient amplification factor (η_1) can be computed by dividing the maximum measured bending moment computed in the transient phase ($M_{\max-transient}$) and pre-liquefaction ($M_{pre-liq}$) condition:

$$\eta_1 = \frac{M_{\max-transient}}{M_{pre-liq}} \tag{1}$$

The transient amplification factor (η_2) can be computed by dividing the maximum bending moment in the transient phase ($M_{\max-transient}$) to that computed at full liquefaction ($M_{post-liq}$):

$$\eta_2 = \frac{M_{\max-transient}}{M_{post-liq}} \tag{2}$$

The transient amplification factors were computed for all the tests listed in Table 3. For each of the 4 pile models, these factors were calculated for all the levels where bending strain was recorded (4 levels for SP1 and GP1, and 7 levels for SP2 and GP2, see Fig. 3 for the experimental layout). The experimental transient amplification factors were plotted for parameters such as time to reach liquefaction (t_{liq}) and speed of liquefaction (v_{liq}).

Fig. 9 presents the effect of time taken to reach full liquefaction on transient amplification factors η_1 & η_2. In this figure, the results from this research are compared with results obtained by applying white noise input motion (WN-1 in Table 3), in which the time taken to liquefy the soil was intentionally lengthened to about 50s., which is significantly higher than that required when more realistic input motions are applied, which is typically around 10s. It is also observed that for a particular pile model, the transient amplification factor increases with increasing time to liquefaction; this suggests that the longer the duration of the transient phase the greater the amplification of the bending moment. Furthermore, as the time taken to reach liquefaction increases, there is more possibility for the pile model time period to become tuned with that of the input motion, thus resulting in a prolonged resonance phenomenon.

Fig. 10 presents the effect of speed of liquefaction t_{liq} (defined in Table 4) on the transient amplification factors (η_1 & η_2). It can be seen that the transient amplification factor decreases with increasing the speed of liquefaction, confirming the conclusions drawn from Fig. 9, discussed earlier.

Fig. 11 plots the transient amplification factors η_1 and η_2 versus the time period elongation ratio, defined as the ratio of time period in post liquefaction ($T_{post-liq}$) to time period in pre liquefaction ($T_{pre-liq}$). It can be noted that both amplification factors increase with increasing time

Table 4
Parameters and non-dimensional groups.

Physical Meaning	Definition	Remarks
Amplification of bending moment in the transient stage as compared to pre-liquefaction and post-liquefaction stage. This factor is nondimensional.	$\eta_1 = \frac{M_{\max-transient}}{M_{pre-liq}}$ $\eta_2 = \frac{M_{\max-transient}}{M_{post-liq}}$ $M_{pre\text{-}liq}$ is maximum bending moment in pile in pre-liquefaction stage based on p-y curves shown in Fig. 2b. $M_{post\text{-}liq}$ is the maximum bending moment in the pile in post-liquefaction stage based on p-y curves shown in Fig. 2c.	**T**ransient **A**mplification **F**actor for dynamic bending moment (TAF). In the absence of more detailed rigorous work, one can estimate the design bending moment by using the model shown in Fig. 2.
Elongation of period of the structure due to liquefaction. This factor is nondimensional.	$\frac{T_{post-liq}}{T_{pre-liq}}$ $T_{post\text{-}liq}$ is the period of the structure at full liquefaction. $T_{pre\text{-}liq}$ is the period of the structure at full liquefaction.	This parameter quantifies the increase in flexibility due to liquefaction
Time taken to reach full/ maximum liquefaction This factor has dimension of time and is measured in s.	t_{liq}	This also quantify the time taken to substantially increase the flexibility of the structure. It may be noted that this parameter can be estimated using commercially available FE software programs
Velocity of liquefaction front This parameter has the unit of length over time and is normally measured in m/s.	$v_{liq} = \frac{D_l}{t_{liq}}$	D_l is the maximum depth of liquefaction i.e. the depth to which the ground liquefies. This parameter can be estimated from the time taken by the soil deposit to liquefy.
Non-dimensional transient dynamics factor This factor is nondimensional.	$\frac{t_{liq}}{T_{pre-liq}}$	This non-dimensional parameter reflects the process of transient as it involves the duration of the transient phase, as well as the initial period of the structure.

period elongation ratio ($\frac{T_{post-liq}}{T_{pre-liq}}$), which implies longer time to reach the onset of liquefaction.

As the responses of free-headed and fixed headed piles are different, transient amplification factors were investigated separately for free-headed pile (i.e. single pile) and fixed headed pile (i.e. pile group) as shown in Figs. 12–14. The TAF were plotted versus non-dimensional transient dynamics parameter given by $\frac{t_{liq}}{T_{pre-liq}}$. Fig. 12 shows that higher amplification factor was computed at mid-depths for free headed pile models, whereas for fixed-headed pile, deep elevations showed larger amplification.

As the difference between η_1 and η_2 for free-headed and fixed-headed pile were not significant, these two factors can be combined and plotted together. Fig. 14 shows the amplification factor η computed for free-headed and fixed headed piles. Despite the scatter in the experimental data, a pattern emerged when performing a liner regression (solid line) and computing the 95% interval. More specifically, it can be seen that that the amplification factor increased with increasing time to liquefaction. Furthermore, it is interesting to reanalyze the two case studies introduced earlier in section 3.2 by computing the non-dimensional transient dynamic ratio $\frac{t_{liq}}{T_{pre-liq}}$. It can be seen that for Showa Bridge, t_{liq} is 10s and T_{pre_liq} is 2s, hence the non-dimensional ratio is 5, which from Fig. 14a and assuming free-headed condition corresponded to an amplification of about 2.5. On the other hand, the corresponding values for the 5-story building in Kobe, these are $t_{liq} = 6$ and $T_{pre} = 0.5$s, corresponded to an amplification of about 3.5.

As the time to liquefaction is not always available, further statistical analyses show that the distribution of the amplification factor follows a Gumbel distribution, with mean value η around 3 for both free and fixed headed piles (see Fig. 15). It is therefore recommended that in the absence of detailed analysis and during preliminary design phase, a value of 3 may be used for TAF for the calculation of the bending moment in the transition phase.

4. Discussion and conclusion

A series of shake table tests have been carried out to understand the transient dynamic behaviour of pile supported structures, particularly when the structure transits from no-liquefaction to full liquefaction. The tests show that the soil liquefies progressively from top to bottom. The velocity of the propagation front is dependent on the characteristics of the input motion and the ground profile. As soil liquefies, the time period of the structure progressively increases owing to the increased flexibility, and in this process the natural frequency of the system may tune with the predominant frequencies of the earthquake, resulting in an amplified response. During liquefaction, the bending moment in the pile constantly changes not only with depth but also with time due to amplification of responses owing to dynamic effects, such as resonance. It is observed that the maximum bending moment in the pile may occur in the transient phase. It is further noted that if the time taken to liquefaction is longer, higher is the amplification of bending moment in the transient phase, the latter is the design bending moment.

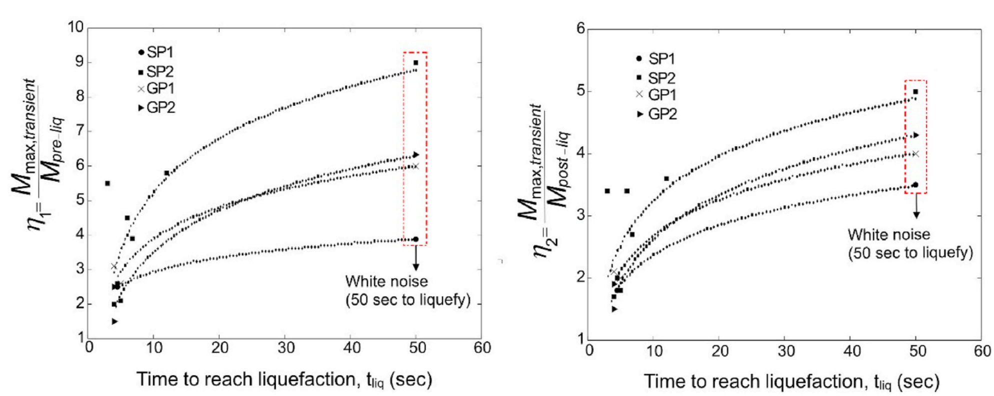

Fig. 9. Time to reach liquefaction vs transient amplification factors η_1 and η_2.

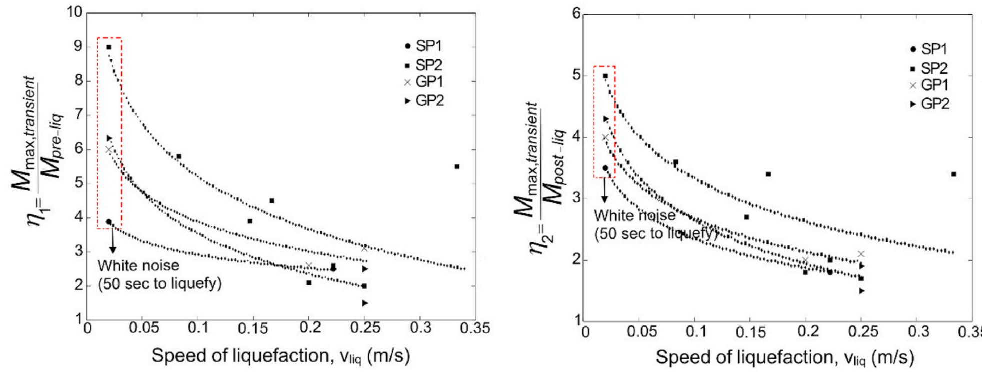

Fig. 10. Speed of liquefaction vs transient amplification factors η_1 and η_2.

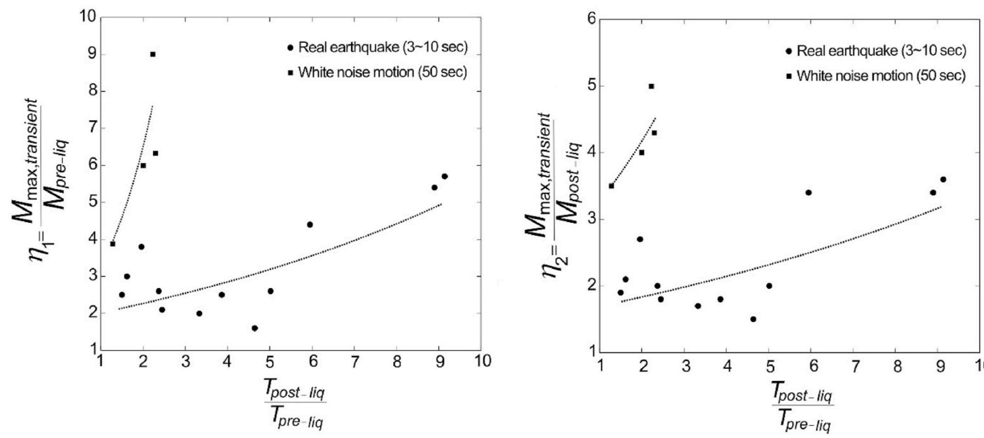

Fig. 11. Transient amplification factors (η_1 and η_2) versus percentage of stiffness.

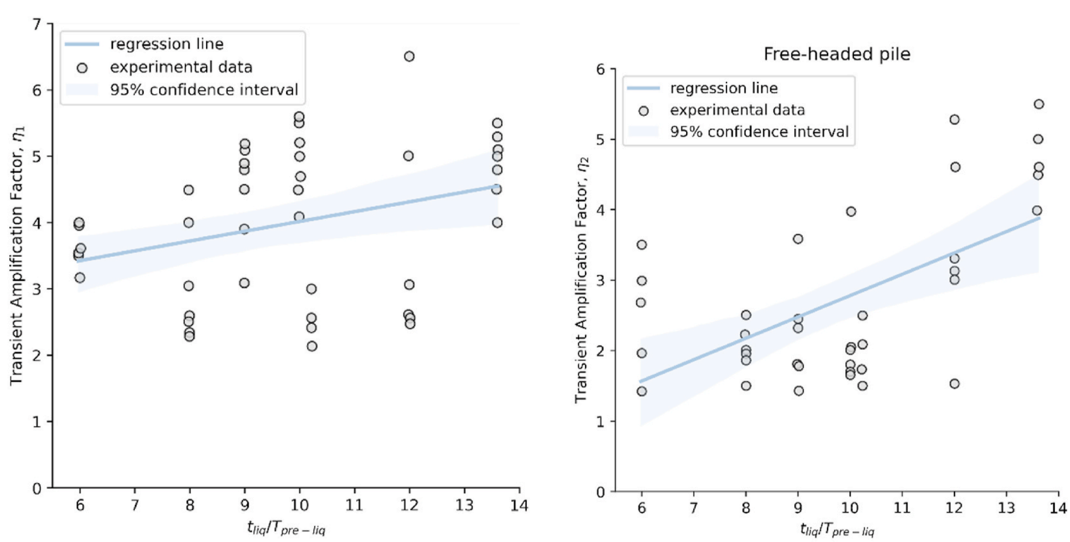

(a) (b)

Fig. 12. Transient amplification factors η_1 and η_2 versus: a) amplification factor with respect to pre-liquefaction condition; b) amplification with respect to liquefaction condition.

The tests results are analysed through a non-dimensional framework which can conveniently be used for design calculations. The non-dimensional parameters consider the elongation of the time period of the structure due to liquefaction and amplification of bending moment. It is shown that dynamic amplification of the bending moment during the transient phase are caused by complex non-linear processesinvolving different mechanisms whose governing parameters can be attributed to the following:

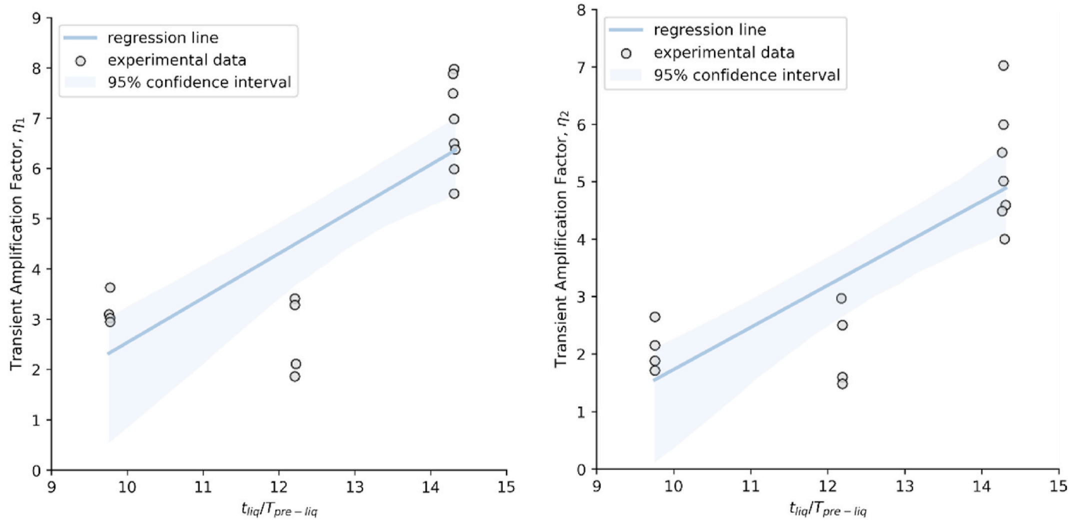

Fig. 13. Transient amplification factors η_1 and η_2 versus $\frac{t_{liq}}{T_{pre-liq}}$: a) amplification factor with respect to pre-liquefaction condition; b) amplification with respect to liquefaction condition.

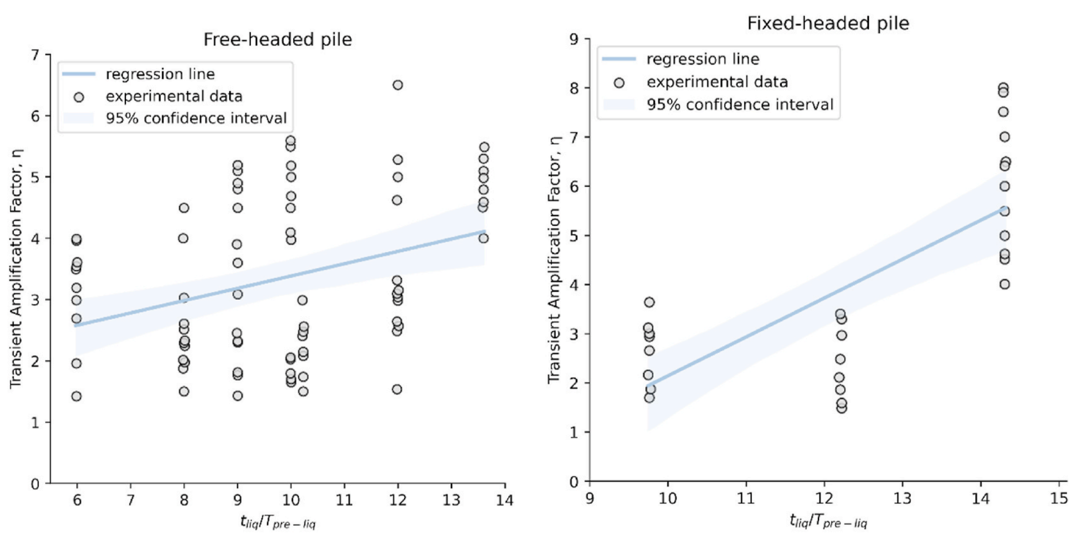

(a) (b)

Fig. 14. Transient amplification factor (η) versus $\frac{t_{liq}}{T_{pre-liq}}$: (a) free-headed pile; (b) fixed headed pile.

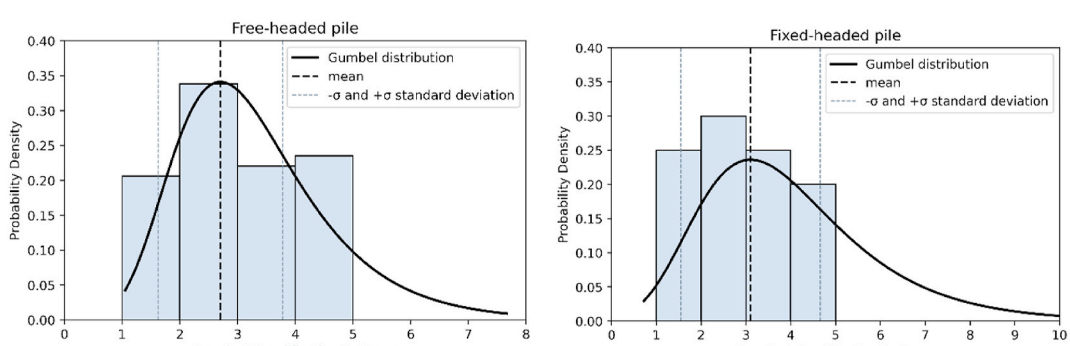

(a) *(b)*

Fig. 15. Probability density distribution of transient amplification factor η and mean values a) free-headed pile; (b) fixed headed pile.

(a) Lengthening of the natural period of the structure ($T_{pre\text{-}liq}$ and $T_{post\text{-}liq}$);
(b) Frequency content of the earthquake, which changes during the transient phase;
(c) Speed of liquefaction front, or in other words, the time taken to transit from pre-liquefaction to post-liquefaction stage;
(d) Variation of system's damping due to excess pore water pressure build-up.

Based on these arguments, it can be concluded that the transient bending moment experienced by the pile depends on the input motion characteristics (i.e., frequency content and amplitude), change in natural period of the pile-supported structure from pre-to full liquefaction conditions, and duration of the transient phase.

The design bending moment for the pile can be estimated by multiplying the maximum predicted bending moment at pre- and post-liquefaction stage by a factor referred to as TAF (Transient Amplification Factor for dynamic bending moment). It is demonstrated that TAF depends on the non-dimensional transient dynamic parameter $\frac{t_{liq}}{T_{pre-liq}}$, given by the ratio of time taken to liquefaction t_{liq} to initial natural period of the structure $T_{pre\text{-}liq}$. As damping of a real system cannot be scaled, use of TAF in design practice needs further thought and further work is required. However, in the absence of other data, and in preliminary design stage, the bending moment can be amplified by a factor of about 3 to take into account the dynamic effects experienced by the foundation during the transient to liquefaction stage.

Author statement

The experimental work done by MR and DL. The analysis and writing is done by MR and DL. The concept of the work and editing is done by SB.

Declaration of competing interest

The authors declare that they have no known competing financial interests or personal relationships that could have appeared to influence the work reported in this paper.

Acknowledgment

The authors are grateful to the Engineering and Physical Science and Research Council (grant EP/H015914/2) for the financial support provided for the present study.

Appendix – A. Mechanics based scaling

The design and interpretation of small-scale models require the assessment of a set of laws of similitude that relate the model to the prototype structure. These can be derived from differential equations and/or dimensional analysis from the assumptions that every physical process can be expressed in terms of non-dimensional groups and the fundamental aspects of physics must be preserved in the design of model tests. Given the premise that strong earthquakes are infrequent, and that most foundations are not instrumented, there is little opportunity for studying the seismic response of piled foundations during liquefaction in full scale testing. Consequently, physical modelling provides an opportunity for understanding the complex soil-structure interaction in a well-controlled laboratory conditions. In this study a series of shake table tests were carried out to investigate of the transient vibration characteristics of pile group models during liquefaction. The necessary steps associated with designing such a model can be stated as follows:

(1) **STEP -1**: What are the potential failure mechanisms or processes that are likely to occur? In other words, what are we trying to find? Care needs to be taken for the cases where ones a priori assumptions preclude certain system behavior of potential interest in the prototype. In the current context, the motivation is the effect of rate of liquefaction on pile response i.e. what is more damaging if the ground liquefies to the maximum slowly or rapidly. This step is PHYSICS or MECHANICS based.
(2) **STEP-2**: Deduction of the relevant non-dimensional groups for the identified mechanisms or processes in Step-1. This is provided in Table 4 and the crucial non-dimensional group is $\frac{t_{liq}}{T_{pre-liq}}$ which is the ratio of time to reach maximum liquefaction (t_{liq}) to the time-period of the structure prior to liquefaction ($T_{pre\text{-}liq}$).
(3) **STEP-3**: Ensure that the set of crucial scaling laws (which are essential) are simultaneously conserved between model and prototype through pertinent similitude relationships. This is ensured through back analyzing of field case records and two examples are taken here.

Example Prototype-1. For widely studied collapse of Showa Bridge during 1964 Niigata earthquake, see Bhattacharya et al. [54] time to reach liquefaction (t_{liq}) is 10s and time period of the bridge pre-liquefaction (T_{pre_liq}) is 2s. Hence the non-dimensional ratio $\frac{t_{liq}}{T_{pre-liq}}$ is 5.

Example Prototype-2. A 5-story building in Kobe and studied in Bhattacharya and Goda [13] and Bhattacharya [57], $t_{liq} = 6$ and $T_{pre_liq} = 0.5$s. Hence the ratio $\frac{t_{liq}}{T_{pre-liq}}$ is 12.

(4) **STEP-4**: In the tests, $\frac{t_{liq}}{T_{pre-liq}}$ was maintained to make the results meaningful. Furthermore, it is necessary to identify scaling laws that are approximately satisfied, and those which are violated, and which therefore require special consideration. Example of the latter are stiffness and dilatancy of soils in 1-g testing.

Once the non-dimensional groups are identified, scaled tests need to be designed to check the non-linearity amongst those groups. These non-dimensional groups can later be used to develop design charts and approximate/simplified design rules. The following sections describe the scaling laws employed for the design of the small-scale models and interpretation of the experimental results, experimental setup and testing programme.

APPENDIX – B

Data from other tests.

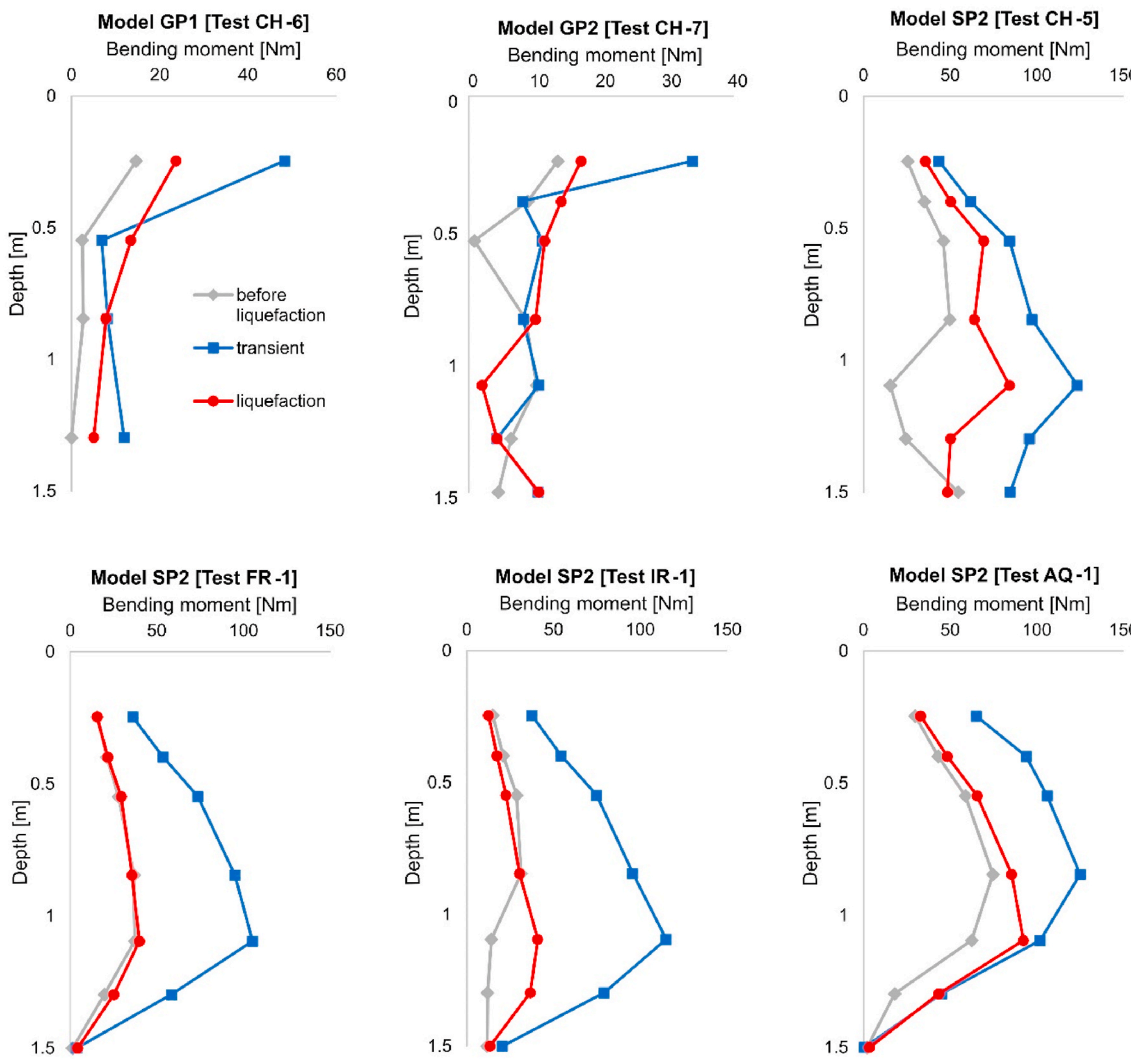

Fig. A-1. Bending moment envelopes for models GP1 (test ID: CH6), GP2 (test ID: CH7), SP2 (test ID: CH5), SP2 (test ID FR-1), SP2 (test ID IR-1) and SP2 (test ID AQ1).

References

[1] Xu C, Dou P, Du X, El Naggar MH, Miyajima M, Chen S. Seismic performance of pile group-structure system in liquefiable and non-liquefiable soil from large-scale shake table tests. Soil Dynam Earthq Eng 2020:138. https://doi.org/10.1016/j.soildyn.2020.106299.

[2] Sawamura Y, Inagami K, Nishihara T, Kosaka T, Hattori M, Kimura M. Seismic performance of group pile foundation with ground improvement during liquefaction. Soils Found 2021;61(4):944–59. https://doi.org/10.1016/j.sandf.2021.06.010.

[3] Li X, Tang L, Man X, Qiu M, Ling X, Cong S, Elgamal A. Liquefaction-induced lateral load on pile group of wharf system in a sloping stratum: a centrifuge shake-table investigation. Ocean Eng 2021:242. https://doi.org/10.1016/j.oceaneng.2021.110119.

[4] Tang L, Man X, Zhang X, Bhattacharya S, Cong S, Ling X. Estimation of the critical buckling load of pile foundations during soil liquefaction. Soil Dynam Earthq Eng 2021;146. https://doi.org/10.1016/j.soildyn.2021.106761.

[5] Hussein AF, El Naggar MH. Seismic axial behaviour of pile groups in non-liquefiable and liquefiable soils. Soil Dynam Earthq Eng 2021;149. https://doi.org/10.1016/j.soildyn.2021.106853.

[6] Hall FE, Lombardi D, Bhattacharya S. Identification of transient vibration characteristics of pile-group models during liquefaction using wavelet transform. Eng Struct 2018 Sep 15;171:712–29.

[7] Su L, Tang L, Ling X, Lui C, Zhang X. Pile response to liquefaction-induced lateral spreading: a shake-table investigation. Soil Dynam Earthq Eng 2016;82:196–204.

[8] Lombardi D, Bhattacharya S. Evaluation of seismic performance of pile-supported models in liquefiable soil. Earthq Eng Struct Dynam 2016;45:1019–38.

[9] Lombardi D, Bhattacharya S. Liquefaction of soil in the Emilia-Romagna region after the 2012 Northern Italy earthquake sequence. Nat Hazards 2014 Sep 1;73(3):1749–70.

[10] Chen Y, Xu C, Liu H, Zhang W. Physical modeling of lateral spreading induced by inclined sandy foundation in the state of zero effective stress. Soil Dynam Earthq Eng 2015;76:80–5.

[11] Tang L, Ling X. Response of a RC pile group in liquefiable soil: a shake-table investigation. Soil Dynam Earthq Eng 2014;67:301–15.

[12] Motamed R, Towhata I, Honda T, Tabata K, Abe A. Pile group response to liquefaction-induced lateral spreading: E-Defense large shake table test. Soil Dynam Earthq Eng 2013;51:35–46.

[13] Bhattacharya S, Goda K. Probabilistic buckling analysis of axially loaded piles in liquefiable soils. Soil Dynam Earthq Eng 2013;45:13–24.

[14] Gao X, Ling X, Tang L, Xu P. Soil–pile-bridge structure interaction in liquefying ground using shake table testing. Soil Dynam Earthq Eng 2011;31:1009–17.

[15] Chau KT, Shen CY, Guo X. Nonlinear seismic soil–pile–structure interactions: shaking table tests and FEM analyses. Soil Dynam Earthq Eng 2009;29:300–10.

[16] Dungca JR, Kuwano J, Takahashi A, Saruwatari T, Izawa J, Suzuki H, Tokimatsu K. Shaking table tests on the lateral response of a pile buried in liquefied sand. Soil Dynam Earthq Eng 2006;26:287–95.

[17] Cubrinovski M, Kokusho T, Ishihara K. Interpretation from large-scale shake table tests on piles undergoing lateral spreading in liquefied soils. Soil Dynam Earthq Eng 2006;26:275–86.

[18] Tokimatsu K, Suzuki H, Sato M. Effects of inertial and kinematic interaction on seismic behaviour of pile with embedded foundation. Soil Dynam Earthq Eng 2005;25:753–62.

[19] Finn WDL, Fujita N. Piles in liquefiable soils: seismic analysis and design issues. Soil Dynam Earthq Eng 2002;22:731–42.

[20] Finn WDL, Thavaraj T. Deep foundations in liquefiable soils: case histories, centrifuge tests and methods of analysis. In: Proceedings of the 4th International

Conference on recent advances in geotechnical earthquake engineering and soil dynamics and Symposium in Honour of Professor W.D. Liam Finn. San Diego, California; 2001. March 26-31.
[21] Dash S. Lateral pile-soil interaction in liquefiable soils. PhD *thesis*. University of Oxford; 2013.
[22] Li Gangjin, Motamed Ramin. Finite element modeling of soil-pile response subjected to liquefaction induced lateral spreading in a large-scale shake table experiment. Soil Dynam Earthq Eng 2017;92:573–84.
[23] Kamijo N, Saito H, Kusama K, Kontani O, Nigbor R. Seismic tests of pile-supported structure in liquefiable sand using large-scale blast excitation. Nucl Eng Des 2004; 228:367–76. https://doi.org/10.1016/j.nucengdes.2003.06.029.
[24] Lombardi D, Bhattacharya S. Modal analysis of pile supported structures during seismic liquefaction. Earthq Eng Struct Dynam 2014;43:119–38.
[25] Rui Wang, Fu Pengcheng, Zhang Jian-Min. Finite element model for piles in liquefiable ground. Comput Geotech 2016;72:1–14.
[26] Shengzhe Wang, Rolando P. Orense. Modelling of raked pile foundations in liquefiable ground. Soil Dynam Earthq Eng 2014;64:11–23.
[27] Tang L, Ling X, Zhang X, Su L, Liu C, Hui Li H. Response of a RC pile behind quay wall to liquefaction-induced lateral spreading: a shake-table investigation. Soil Dynam Earthq Eng 2015;76:69–79.
[28] Wang X, Ye A, Ji B. Fragility-based sensitivity analysis on the seismic performance of pile-group-supported bridges in liquefiable ground undergoing scour potentials, vol. 198. Engineering Structures; 2019. https://doi.org/10.1016/j.engstruct.2019.109427.
[29] Yu Xu L, Xiang Song C, Chen W, Cai F, Chen G. Liquefaction-induced settlement of the pile group under vertical and horizontal ground motions. Soil Dynam Earthq Eng 2021;144. https://doi.org/10.1016/j.soildyn.2021.106709.
[30] Wang, H. Stuedlein, A.W., Sinha, A. Dynamic response of timber pile ground improvement: 3D numerical simulations. Soil Dynam Earthq Eng. 2021;143. doi: 10.1016/j.soildyn.2021.106614.
[31] Bhattacharya S, Hyodo M, Nikitas G, Ismael B, Suzuki H, Lombardi D, Egami S, Watanabe G, Goda K. Geotechnical and infrastructural damage due to the 2016 Kumamoto earthquake sequence. Soil Dynam Earthq Eng 2018 Jan 1;104:390–4.
[32] JRA. Japanese Road Association. Specification for highway bridges. Part V: seismic design; 1996.
[33] JRA. Japan Road Association. Specifications for highway bridges. Japan: Part V: seismic design; 2002. 2002.
[34] National Earthquake Hazards Reduction Program NEHRP. Commentary (Federal Emergency Management Agency, USA, 369) for seismic regulations for new buildings and other structures. 2000.
[35] IS-1893. Part 1: Criteria for *earthquake resistant* Design of *structures*. New Delhi: Bureau of Indian Standard; 2000.
[36] American Petroleum Institute API. Recommended Practice for *planning,* Designing and *constructing fixed offshore platforms.* Working stress design, API recommended practice 2A-WSD. twenty-first ed. Dallas: RP2A-WSD); 2000.
[37] Bhattacharya S, Madabhushi SPG, Bolton MD. An alternative mechanism of pile failure in liquefiable deposits during earthquakes. Geotechnique 2004;54(3): 203–13.
[38] Bhattacharya S, Rolando PO, Lombardi D. Seismic design of foundations: concepts and applications. ICE Publishing; 2019.
[39] Dobry R, Taboada V, Liu L. Centrifuge modeling of liquefaction effects during earthquakes. In: Proc. 1st Intl. Conf. On earthquake geotechnical engineering. IS-Tokyo; 1995. p. 14–6.
[40] Brandeberg SJ. Behaviour of pile foundations in liquefied and laterally spreading ground. California, USA: Ph.D. Thesis, University of California at Davis; 2005.
[41] Wilson DW, Boulanger RW, Kutter BL. Observed seismic lateral resistance of liquefying sand. J Geotech Geoenviron Eng 2000;126(10):898–906.
[42] Brandenberg SJ, Boulanger RW, Kutter BL, Chang D. Behavior of pile foundations in laterally spreading ground during centrifuge tests. J Geotech Geoenviron Eng 2005;131(11):1378–91.
[43] Yasuda S, Masuda T, Yoshida N, Nagase H, Kiku H, Itafuji S, Mine K, Sato K. Torsional shear and triaxial compression tests on deformation characters of sands before and after liquefaction. In: Proc., 5th US-Japan workshop on earthquake resistant design of lifelines and countermeasures against soil liquefaction; 1994. p. 249–65.
[44] Vaid YP, Thomas J. Liquefaction and post liquefaction behavior of sand. J Geotechn Eng 1995;121(2):163–73.
[45] Lombardi D, Bhattacharya S, Hyodo M, Kaneko T. Undrained behaviour of two silica sands and practical implications for modelling SSI in liquefiable soils. Soil Dynam Earthq Eng 2014;66:293–304.
[46] Lombardi D. Dynamics of pile-supported structures in seismically liquefiable soils. Doctoral dissertation, University of Bristol; 2014.
[47] Lombardi D, Dash SR, Bhattacharya S, Ibraim E, Muir Wood D, Taylor C. Construction of simplified design p-y curves for liquefied soils. Geotechnique 2017: 116. https://doi.org/10.1680/jgeot.15.
[48] Rouholamin M, Bhattacharya S, Orense R. Effect of initial relative density on the post-liquefaction behaviour of sand. Soil Dynam Earthq Eng 2017;97:25–36.
[49] Dash S, Rouholamin M, Lombardi D, Bhattacharya S. A practical method for construction of py curves for liquefiable soils. Soil Dynamics and Earthquake Engineering 2017;97:478–81.
[50] Lombardi D, Bhattacharya S, Scarpa F, Bianchi M. Dynamic response of a geotechnical rigid model container with absorbing boundaries. Soil Dynam Earthq Eng 2015;69:46–56.
[51] Bhattacharya S, Lombardi D, Dihoru L, Dietz MS, Crewe AJ, Taylor CA. Model container design for soil-structure interaction studies. In: *Role of seismic testing facilities in performance-based earthquake engineering.* Dordrecht: Springer; 2012. p. 135–58.
[52] Rouholamin M. An experimental investigation of transient dynamics of pile supported structures in liquefiable soils. PhD *thesis*. UK: University of Surrey; 2016.
[53] Bhattacharya S, Krishna AM, Lombardi D, Crewe A, Alexander N. Economic MEMS based 3-axis water proof accelerometer for dynamic geo-engineering applications. Soil Dynam Earthq Eng 2012;36:111–8. https://doi.org/10.1016/j.soildyn.2011.12.001.
[54] Bhattacharya S, Tokimatsu K, Goda K, Sarkar R, Shadlou M, Rouholamin M. Collapse of Showa Bridge during 1964 Niigata earthquake: a quantitative reappraisal on the failure mechanisms. Soil Dynam Earthq Eng 2014;65:55–71.
[55] Haldar S, Sivakumar Babu GL. Effect of soil spatial variability on the response of laterally loaded pile in undrained clay. Comput Geotech 2008;35:537–47.
[56] Bhattacharya S, Madabhushi SPG. A critical review of methods for pile design in seismically liquefiable soils. Bull Earthq Eng 2008;6(3):407–46. https://doi.org/10.1007/s10518-008-9068-3.
[57] Bhattacharya S. Safety assessment of existing piled foundations in liquefiable soils against buckling instability. ISET J Earthq Technol 2006;43(4):133–47.